

Radiative association of C(³P) and H⁺: Triplet States

James F. Babb^{1*} and Brendan M. McLaughlin^{1,2†}

¹*Institute for Theoretical Atomic Molecular and Optical Physics (ITAMP), Harvard-Smithsonian Center for Astrophysics, 60 Garden St., Cambridge, MA 02138, USA*

²*Center for Theoretical Atomic Molecular and Optical Physics (CTAMOP), School of Mathematics and Physics, The David Bates Building, 7 College Park, Queens University Belfast, Belfast BT7 1NN, UK*

Accepted XXX. Received YYY; in original form: 13 March 2017

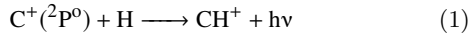
ABSTRACT

The radiative association of C(³P) and H⁺ is investigated by calculating cross sections for photon emission into bound ro-vibrational states of CH⁺ from the vibrational continua of initial triplet d³Π or b³Σ⁻ states. Potential energy curves and transition dipole moments are calculated using multi-reference configuration interaction (MRCI) methods with AV6Z basis sets. The cross sections are evaluated using quantum-mechanical methods and rate coefficients are calculated. The rate coefficients are about 100 times larger than those for radiative association of C⁺(²P^o) and H from the A¹Π state. We also confirm that the formation of CH⁺ by radiative association of C⁺(²P^o) and H via the triplet c³Σ⁺ state is a minor process.

Key words: ISM:molecules – molecular processes – astrochemistry – molecular data – scattering

1 INTRODUCTION

The methylidyne ion CH⁺ (methylidyne) is a prominent interstellar molecular ion and the mechanisms of its formation in various astrophysical environments continue to be of interest (Black & Dalgarno 1973; Stecher & Williams 1974; Dalgarno & Black 1976; Talbi & DeFrees 1991; Williams 1992; Tielens 2005; Indriolo et al. 2010; Nagy et al. 2013; Bacchus-Montabonel & Wiesenfeld 2013; Morris et al. 2016). In particular, the formation of CH⁺ by radiative association of C⁺ and H,

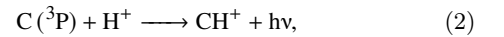


was explored using collision theory some time ago by Bates (1951) and in subsequent improved calculations (Solomon & Klemperer 1972; Smith et al. 1973; Giusti-Suzor et al. 1976; Graff et al. 1983; Barinovs & van Hemert 2006). No calculations, however, yielded a rate coefficient for the process (1) that was large enough to explain the observed abundance of CH⁺ in diffuse interstellar clouds (Giusti-Suzor et al. 1976; Barinovs & van Hemert 2006) and, depending on the application, other formation mechanisms are now considered of more significance (Black & Dalgarno 1973; Dalgarno & Black 1976; Black & Dalgarno 1977; Stecher & Williams 1974; Williams 1992; Cecchi-Pestellini 2010; Nagy et al. 2013).

Prior studies of the reaction (1) considered transitions of the singlet symmetry molecular states A¹Π → X¹Σ⁺ for

the radiative association process in C⁺(²P^o) and H collisions, as the c³Σ⁺ → a³Π transitions are expected to be insignificant (Giusti-Suzor et al. 1976). In Fig. 1 the potential energy curves of CH⁺ correlating to C⁺(²P^o)+H are shown. The most recent calculations find that the rate coefficient for the radiative association process (1) is about ~ 3 × 10⁻¹⁷ cm³/s at 200 K (Barinovs & van Hemert 2006), only a factor of two smaller than that of Graff et al. (1983).

Another radiative association process leading to CH⁺, for which quantitative data on the rate coefficients are unavailable, is the radiative association of C(³P) atoms and protons



which takes place via initial molecular channels correlating to C(³P) + H⁺ and final channels yielding CH⁺, namely d³Π → a³Π, d³Π → b³Σ⁻, and b³Σ⁻ → a³Π, as illustrated in Fig. 1. Inspection of Fig. 1 reveals that the triplet transition d³Π → c³Σ⁺ is between two repulsive molecular states and does not lead to significant bound CH⁺. Stancil et al. (1998a) assessed radiative collisions between C(³P)+H⁺ leading to C⁺(²P^o)+H, but detailed calculations for the radiative association process (2) are not available. In the present paper, we calculate, using quantum-mechanical collision theory, the cross sections and rate coefficients for the radiative association process (2) via the d³Π → a³Π, d³Π → b³Σ⁻, and b³Σ⁻ → a³Π transitions. For completeness, we also assess quantitatively the c³Σ⁺ → a³Π transitions and confirm their insignificance for radiative association.

* E-mail: jabb@cfh.harvard.edu

† E-mail: bmclaughlin899@btinternet.com

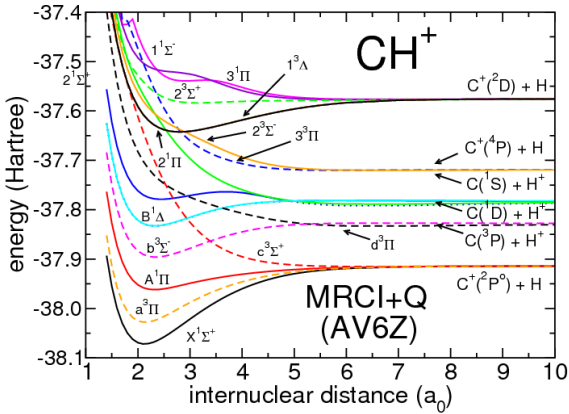


Figure 1. Potential energy curves for CH^+ ; singlet (solid lines) and triplet molecular states (dashed lines) as a function of internuclear distance. All quantities are in atomic units (1 Hartree = $e^2/a_0 \approx 27.2114$ eV).

2 THEORY

The quantum mechanical theory of radiative association is well-established. The cross section $\sigma_{i \rightarrow f}(E)$ for the process can be calculated using perturbation theory, see for example (Stancil et al. 1993; Nyman et al. 2015),

$$\sigma_{i \rightarrow f}(E) = \sum_{v'J'} \sum_J \frac{64 \pi^5 \hbar^2}{3} \frac{\nu^3}{c^3} \frac{1}{2\mu E} P_i S_{JJ'} |M_{iEJ, f\nu'J'}|^2, \quad (3)$$

where the sum is over the initial rotational J , final vibrational v' , and rotational J' quantum numbers, i and f , respectively, denote the initial and final electronic states, and $h\nu = E + |E_{\nu'J'}|$ is the photon energy. The cross sections depend on the relative kinetic energy $E = \hbar^2 k^2 / 2\mu$ of the $\text{C}(^3\text{P})$ and H^+ (or in the case of the $\text{c}^3\Sigma^+ - \text{a}^3\Pi$ states the $\text{C}^+(^2\text{P}^0)$ and H) colliders, with momentum $\hbar k$, where μ is the reduced mass. The statistical weight factors P_i are $\frac{2}{3}$ for the $\text{d}^3\Pi$ state, $\frac{1}{3}$ for $\text{b}^3\Sigma^-$ state, and $\frac{1}{4}$ for $\text{c}^3\Sigma^+$ state, $S_{J,J'}$ are the appropriate line strengths (Cowan 1981; Curtis 2003) or Hönl-London factors (Watson 2008), and c is the speed of light. The matrix element $M_{iEJ, f\nu'J'}$ is given by the integral

$$M_{iEJ, f\nu'J'} = \int_0^\infty F_{iEJ}(R) D(R) \Phi_{f\nu'J'}(R) dR, \quad (4)$$

where the wave function $\Phi_{f\nu'J'}(R)$ is a bound state eigenfunction on the final electronic state, $D(R)$ is the transition dipole moment function, and $F_{iEJ}(R)$ is an energy-normalized continuum wave function on the initial electronic state. The bound and continuum state wave functions may be computed from their respective Schrödinger equations (Mott & Massey 1965) using standard methods (Cooley 1961; Johnson 1977).

Rate coefficients are calculated by averaging the cross section over a Maxwellian velocity distribution and are given

by

$$\alpha(T) = \left(\frac{8}{\pi\mu}\right)^{1/2} \left(\frac{1}{k_B T}\right)^{3/2} \int_0^\infty E \sigma_{i \rightarrow f}(E) \exp\left(-\frac{E}{k_B T}\right) dE, \quad (5)$$

where k_B is the Boltzmann constant.

3 CALCULATIONS

3.1 Molecular Structure

The low-lying potential energy curves of CH^+ , $\text{X}^1\Sigma^+$ and $\text{A}^1\Pi$, have been extensively studied, see, for example, Elander et al. (1977); Saxon et al. (1980) and the summary in Cho & Le Roy (2016). Detailed calculations have also been performed for the excited $\text{a}^3\Pi$ and $\text{c}^3\Sigma^+$ states by Green et al. (1972); Graff et al. (1983); Barinovs & van Hemert (2004); O'Connor et al. (2016).

Extended calculations provide information on the $\text{b}^3\Sigma^-$ state (Saxon & Liu 1983) and the $\text{d}^3\Pi$ state correlating to $\text{C}(^3\text{P}) + \text{H}^+$ (Levy et al. 1985; Stancil et al. 1998a; Biglari et al. 2014). Other recent sophisticated calculations include the quasi-degenerate many body perturbation theory (MBPT) approach of Kanzler et al. (1991), the equation of motion coupled cluster (EOMCCSDT) method developed by Kowalski & Piecuch (2001), the multi-reference perturbation theory (MRPT) used by Seleznev & Khurstov (2012); Seleznev et al. (2013), and the effective (mass-dependent) calculations of Sauer & Špirko (2013).

In order to perform dynamical calculations for the radiative association cross sections and rates for process (2), we require the potential energy curves (PECs) for the triplet states of the entrance and exit channels, and the transition dipole moment (TDM) coupling the states.

Some of the necessary data are available in the literature mentioned above. In particular, Biglari et al. (2014) used the quantum chemistry suites ORCA and GAMESS-US in multi-reference configuration interaction (MRCI) calculations with aug-cc-pV5Z (AV5Z) basis sets. We chose to calculate the potential energy curves and transition dipole moments using the MRCI approach with the MOLPRO quantum chemistry suite, using AV6Z basis sets. In MOLPRO, we use C_{2v} symmetry with the order of Abelian irreducible representations being (A_1, B_1, B_2, A_2) . In reducing the symmetry from $\text{C}_{\infty v}$ to C_{2v} , the correlating relationships are $\sigma \rightarrow a_1$, $\pi \rightarrow (b_1, b_2)$, and $\delta \rightarrow (a_1, a_2)$. We employed the non-relativistic state-averaged complete-active-space-self-consistent-field (SA-CASSCF)/MRCI method (Werner & Knowles 1985; Knowles & Werner 1985), available within the MOLPRO quantum chemistry codes (Werner et al. 2015), to take account of short-range interactions. In detail, for this cation, six molecular orbitals (MOs) are put into the active space, including four a_1 , one b_1 and one b_2 symmetry MO's with all electron active. The molecular orbitals for the MRCI procedure were obtained from the state-averaged-multi-configuration-self-consistent-field (SA-MCSCF) method. In our work the Davidson correction (+Q) (Langhoff & Davidson 1974) was also applied to all molecular states. The averaging processes is carried out for the lowest five (1A_1), five (1B_1), five (1A_2), five (3A_1), five (3B_1), and five (3A_2) molecular states of the molecular ion in C_{2v} .

Table 1. Equilibrium bond distance R_e (Å) and dissociation energies D_e (eV) for the X ¹Σ⁺, a ³Π, A ¹Π and b ³Σ⁻ states of CH⁺ for the present MRCI+Q calculations compared to other theoretical and experimental results. (The data are given in units conventional to quantum chemistry with 1 Å=10⁻¹⁰ m and 0.529177 Å ≈ a₀.)

State	Method	$R_e/\text{Å}$	D_e/eV
X ¹ Σ ⁺	MRCI+Q ^a	1.1256	4.291
	MRCISD ^b	1.130	4.244
	MCSCF+CI ^c	1.1290	4.140
	QD-MBPT ^d	1.1250	4.66
	MRD-CI ^e	1.129	4.01
	EOMCCSDt ^f	1.1404	–
	Experiment ^g	1.1308843(30)	4.77(43)
	Empirical ^h	1.1284625(58)	4.26044(4)
	a ³ Π	MRCI+Q ^a	1.1305
MRCISD ^b		1.135	3.0404
QD-MBPT ^d		1.1473	3.44
MRD-CI ^e		1.135	2.88
EOMCCSDT ^f		1.1261	3.4404
Experiment ⁱ		1.1348	–
A ¹ Π		MRCI+Q ^a	1.2264
	MRCISD ^b	1.2390	1.239
	MCSCF+CI ^c	1.2600	0.9360
	QD-MBPT ^d	1.2055	1.53
	MRD-CI ^e	1.243	1.00
	Experiment ⁱ	–	1.2785
	Empirical ^h	1.235896(14)	1.27750(3)
b ³ Σ ⁻	MRCI+Q ^a	1.2373	1.855
	MRCISD ^b	1.244	1.833
	MCSCF+CI ^c	1.2452	1.854
	MRD-CI ^e	1.245	1.80
	Experiment ⁱ	1.2416	–

^aMulti-reference configuration interaction (MRCI) and Davidson correction (+Q), aug-cc-pV6Z basis, present work

^bMRCI with all single (S) and double (D) excitations, (MRCISD), aug-cc-pV5Z basis (Biglari et al. 2014)

^cMulti-configuration (MC) self-consistent field (SCF) + CI (Saxon et al. 1980; Saxon & Liu 1983)

^dQuasi-Degenerate (QD) many body perturbation theory (MBPT) (Kanzler et al. 1991)

^eMulti-reference (MR) single and double-excitation CI (MRD-CI) (Stancil et al. 1998a)

^fEquation of motion (EOM) coupled cluster (CC) with S, D and triple (T) excitations (Kowalski & Piecuch 2001)

^gExperiment, emission spectroscopy (Hakalla et al. 2006)

^hEmpirical fit of spectroscopic, photodissociation, and translational spectroscopy data (Cho & Le Roy 2016) with energies converted from cm⁻¹ using the factor 1.239842 × 10⁻⁴ eV = 1 cm⁻¹.

ⁱExperiment, photodissociation spectroscopy of stored ions (Hechtfischer et al. 2007)

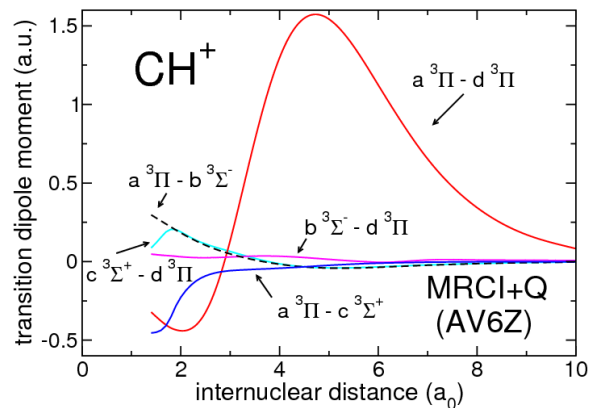


Figure 2. Transition dipole moments for the CH⁺ cation coupling the four low lying triplet molecular states, used in the present radiative association cross section calculations, as a function of internuclear distance. All quantities are in atomic units.

These MOs (4a₁, 1b₁, 1b₂, 0a₂), denoted by (4,1,1,0), were generated from the state-averaging CASSCF process, and used to perform all the subsequent PEC calculations for all the electronic states in the MRCI+Q approximation. Fig. 1 shows the calculated PECs for several low lying singlet and triplet states of the CH⁺ molecular ion as a function of internuclear distance.

Table 1 gives a comparison of the equilibrium bond length R_e , in Å, and the dissociation energy D_e , in eV, determined from our MRCI+Q work for a sample of low-lying states, namely; the X ¹Σ⁺ ground state and the excited a ³Π, A ¹Π, and b ³Σ⁻ states, with the recent MRCI work of Biglari et al. (2014) obtained using an AV5Z basis and with other previous work. Comparison of the present Table 1 with the calculations summarized in Table 2 of Stancil et al. (1998a) confirms that there has been substantial progress in the calculations for these electronic states of CH⁺ in the last two decades. We include the much more precise empirical parameters R_e and D_e for the X ¹Σ⁺ and A ¹Π states from the work of Cho & Le Roy (2016), who analyzed all available spectroscopic, photo-association, and translational spectroscopy data, and who provide a more extensive summary of experimental and theoretical results for these states. Generally, we find that the present calculations yield larger values of D_e and smaller values of R_e than those from Biglari et al. (2014).

Our calculated TDMs are shown in Fig. 2 for the triplet transitions of interest and they are in good agreement with those calculated by others using the MRCISD method (Stancil et al. 1998a; Biglari et al. 2014), where available. The TDM connecting the b ³Σ⁻ state to the d ³Π state is not available, evidently, in the literature and we list our calculated values in Table 2.

As can be seen from Table 1 and Figs. 1–2 our results are in good agreement with other multi-reference CI studies providing further confidence in our molecular data for the dynamical calculations.

Table 2. Transition dipole moment function $D(R)$ between the $b^3\Sigma^-$ state and $d^3\Pi$ state in atomic units. The full table, for $1.4 \leq R \leq 10$, is available at <http://dx.doi.org/10.6084/m9.figshare.4725565>.

R/a_0	$D(R)/e^2 a_0^2$
1.4	0.047740
1.5	0.044145
1.6	0.041119
1.7	0.038630
1.8	0.036429
1.9	0.033665
2.0	0.030672

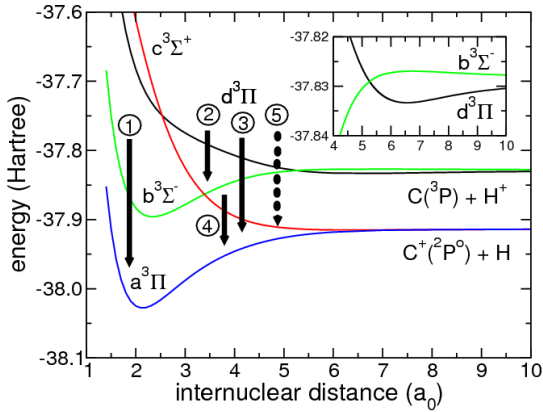


Figure 3. Potential energy curves for the four low-lying triplet molecular states of the CH^+ molecular ion as a function of internuclear distance. The downward pointing solid arrows schematically indicate the transitions studied in the present work for radiative association from: 1) the vibrational continuum of the $b^3\Sigma^-$ state to a bound ro-vibrational level of the $a^3\Pi$ state, and similarly for, 2) $d^3\Pi$ to $b^3\Sigma^-$, 3) $d^3\Pi$ to $a^3\Pi$, and 4) $c^3\Sigma^+$ to $a^3\Pi$ transitions, while, for 5) the dotted line connecting the vibrational continuum of the $d^3\Pi$ state to the vibrational continuum of the $c^3\Sigma^+$ state indicates that radiative charge transfer is the dominant mechanism for this channel. The inset shows the potential energies of the $b^3\Sigma^-$ state and $d^3\Pi$ state at higher energy resolution illustrating the barrier in the $b^3\Sigma^-$ state and the shallow well of the $d^3\Pi$ state. All quantities are in atomic units.

3.2 Cross sections

In the present work, we require only the four low-lying potential energy curves (PECs) for the triplet $a^3\Pi$, $c^3\Sigma^+$, $b^3\Sigma^-$, and $d^3\Pi$ molecular states of Fig. 1, which are plotted in Fig. 3 as a function of internuclear distance. The necessary TDMs for the transitions are illustrated in Fig. 2. It is apparent that the dominant contribution to the radiative association process (2) will come from the $d^3\Pi \rightarrow a^3\Pi$ transition, which has the largest transition dipole moment. Moreover, at initial thermal kinetic energies, the vertical Franck-Condon overlap and relatively small TDMs indicate that the $c^3\Sigma^+ \rightarrow a^3\Pi$ and $d^3\Pi \rightarrow b^3\Sigma^-$ transitions will yield relatively small cross sections compared to the $d^3\Pi \rightarrow a^3\Pi$ transition.

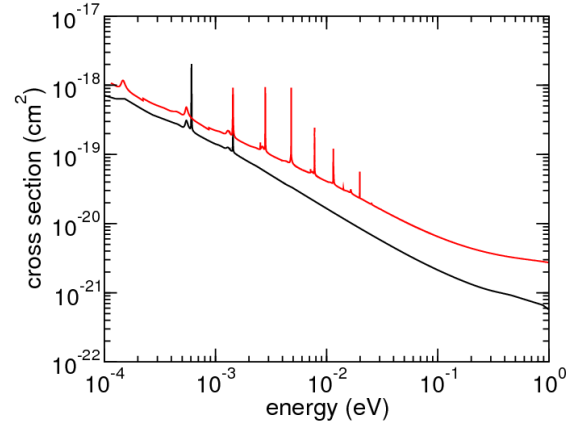


Figure 4. Cross sections (cm^2) for radiative decay (upper, red line) and radiative association (lower, black line) as a function of the collision energy (eV), for the $d^3\Pi \rightarrow a^3\Pi$ transition.

We evaluated equation (3) using the calculated potential energies and TDMs of Sec. 3.1. For values of $R < 1.4 a_0$, we joined the calculated potential energies to the corresponding values for $R = 1.0$ and 1.2 , where available, from Biglari et al. (2014). For $R > 10 a_0$, the appropriate long-range forms were used for the separating atom-ion pair. In particular, for $\text{C}(^3\text{P}) + \text{H}^+$, this corresponds to a R^{-3} quadrupole interaction added to the attractive R^{-4} polarisation potential (Gentry & Giese 1977; Levy et al. 1985). For $\text{C}^+(^2\text{P}^0) + \text{H}$, we used the form $-\frac{1}{2}\alpha_{\text{H}}R^{-4}$, where $\alpha_{\text{H}} = \frac{9}{2}$ is the static electric dipole polarisability of hydrogen. The potential energies for $R < 10$ were adjusted to match the long-range forms at $R = 10$, with the asymptotic energies taken from Table I, column 4, of Stancil et al. (1998a). The TDMs were fit to inverse powers of the internuclear distance for $R > 10$ and extended to $R = 1.0$ and 1.2 using the values, where available, from Biglari et al. (2014).

3.2.1 Triplet states of $\text{C}(^3\text{P})$ and H^+

Our calculated $d^3\Pi$ state is attractive at long-range (Levy et al. 1985; Sarre & Whitham 1988) with a shallow well at about $6.56 a_0$ (see inset, Fig. 3) and the transition dipole moment is large. The radiative association cross sections for the $d^3\Pi$ to $a^3\Pi$ transitions are shown in Fig. 4. For comparison, we calculated the radiative decay cross sections using the distorted wave optical potential approach as detailed by Babb & McLaughlin (2017). The present results for radiative decay generally agree with those of Stancil et al. (1998a); being about a factor two larger than theirs at 10^{-4} eV, though gradually becoming comparable for increasing energies, and being equal for energies above 0.1 eV. The differences may result from the use of different molecular potential energy data. From Stancil et al. (1998a) we can obtain an independent estimate of the radiative association cross sections. We subtracted their radiative charge transfer (denoted full quantum or ‘‘FQ’’) cross sections from their radiative decay cross sections (denoted optical potential distorted wave or ‘‘OPDW’’) given by, respectively, the solid line and dot-

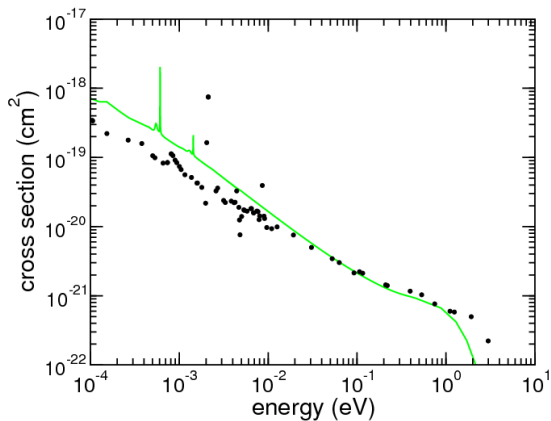


Figure 5. Cross sections for radiative association from the $d^3\Pi$ state to the $a^3\Pi$ state for the present calculation (green line) and estimated (see text) from Stancil et al. (1998a) (black points).

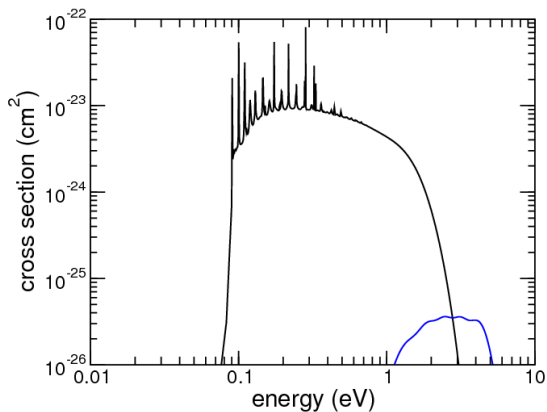


Figure 6. Cross sections (cm^2) as a function of collision energy (eV) for radiative association from the $b^3\Sigma^-$ state to the $a^3\Pi$ state (black line) and from the $d^3\Pi$ state to the $b^3\Sigma^-$ state (blue line).

ted line with points in their Fig. 8. In Fig. 5 we plot the present cross sections and the estimate so obtained and we find the agreement satisfactory for energies above 10^{-2} eV. For lower energies, our values are about twice as large. The discrepancy may arise from the reliability of the subtraction procedure and the different molecular data used.

The cross sections for radiative association for the $b^3\Sigma^-$ to $a^3\Pi$ transitions are shown in Fig. 6. Because the $b^3\Sigma^-$ state is repulsive at long-range see inset, Fig. 3), the cross sections drop off quite rapidly for energies lower than the potential energy local maximum of 0.109 eV (relative to the $C(^3P) + H^+$ limit). Numerous resonances are seen at higher energies; however, as the cross sections are generally small, we did not investigate the resonances in detail. The radiative association cross sections are comparable to the radiative decay cross sections for this channel given in Fig. 8 of Stancil

Table 3. Rate coefficients, in units of cm^3/s , as a function of temperature T , in K, for $d^3\Pi \rightarrow a^3\Pi$ radiative decay and radiative association. A value in parentheses is a power of ten that should multiply the precedent quantity, for example, $1.01(-14)$ represents 1.01×10^{-14} .

$T(K)$	Radiative Decay	Radiative Association
10	1.01(-14)	6.48(-15)
20	9.30(-15)	5.31(-15)
30	8.40(-15)	4.48(-15)
40	7.81(-15)	3.90(-15)
50	7.46(-15)	3.64(-15)
70	6.92(-15)	3.15(-15)
100	6.20(-15)	2.79(-15)
200	5.05(-15)	2.06(-15)
300	4.46(-15)	1.73(-15)
500	3.93(-15)	1.42(-15)
700	3.59(-15)	1.26(-15)
1000	3.35(-15)	1.14(-15)
2000	3.24(-15)	9.87(-16)
3000	3.24(-15)	9.36(-16)
5000	3.45(-15)	8.59(-16)
7000	3.62(-15)	7.72(-16)
10000	3.81(-15)	6.60(-16)

et al. (1998a) but are, however, one hundredth of those for the $d^3\Pi \rightarrow a^3\Pi$ transition.

We also considered the $d^3\Pi \rightarrow b^3\Sigma^-$ transition and the calculated cross sections, shown in Fig. 6, are very small due to limited Franck-Condon overlap. Levels of the $b^3\Sigma^-$ state are predissociated by the $c^3\Sigma^+$ state for $v' \gtrsim 4$, see Hechtfisher et al. (2007) for a detailed analysis, and the probability of forming levels with $v' \leq 4$, which would decay to the $a^3\Pi$ state (Biglari et al. 2014), is small. We ignored predissociation and radiative cascading and estimated the cross sections using the quantum-mechanical approach, Eq. (3), but a more detailed model including predissociation by the $c^3\Sigma^+$ state and radiative decay from the $b^3\Sigma^-$ state to the $a^3\Pi$ state might be warranted.

There is negligible radiative association between the $d^3\Pi$ state and $c^3\Sigma^+$ state because both states are repulsive with shallow long-range wells and the transition dipole moment is small. The cross section can be no more than the radiative decay cross section, for which Stancil et al. (1998a) find about 10^{-21} cm^2 at 10^{-4} eV decreasing to less than 10^{-23} cm^2 at 1 eV.

3.2.2 Triplet states of $C(^2P^0)$ and H

We calculated the cross sections for radiative association from the $c^3\Sigma^+$ to the $a^3\Pi$ state. The values are much smaller compared to those given in the previous section. We find that $\sigma(E)$ is about $8 \times 10^{-28} \text{ cm}^2$ at 10^{-3} eV to about $2 \times 10^{-28} \text{ cm}^2$ at 0.01 eV.

3.3 Rate coefficients

As we have shown, the $d^3\Pi \rightarrow a^3\Pi$ transitions dominate in the radiative association process (2). We calculated the rate coefficients for radiative association and radiative decay using Eq. (5). The results are given in Table 3.

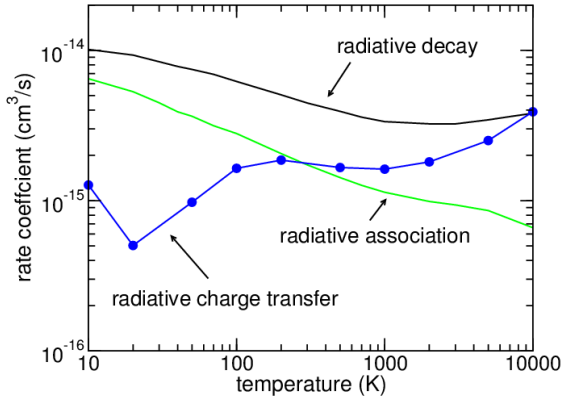


Figure 7. For the $d^3\Pi \rightarrow a^3\Pi$ transition, the present rate coefficients for radiative association and radiative decay compared to the rate coefficients from Stancil et al. (1998b) for radiative charge transfer (dots with guide line).

The sum of the rate coefficients for the radiative association and the radiative charge transfer processes should be approximately equal to the rate coefficients for radiative decay (Cooper et al. 1984). As an additional check of our results, we examined the temperature dependence of the present radiative association and radiative decay rate coefficients and the radiative charge transfer rate coefficients of Stancil et al. (1998b) (who used using a different set of molecular data), see Fig. 7. With increasing temperature, the radiative association rate coefficient diminishes and the radiative charge transfer coefficient increases, but their sum remains close to the radiative decay rate coefficient.

We fit the calculated rate coefficients to the formula (Novotný et al. 2013; Vissapragada et al. 2016)

$$\alpha(T) = a(300/T)^x + T^{-3/2} \sum_{i=1}^3 c_i \exp(-d_i/T) \text{ cm}^3/\text{s}, \quad (6)$$

with T expressed in K. For radiative decay ($d^3\Pi \rightarrow a^3\Pi$), the values are $a = 4.89675 \times 10^{-15}$, $x = 0.1797$, $c_1 = 7.35952 \times 10^{-9}$, $d_1 = 18087.6$, $c_2 = -3.38159 \times 10^{-11}$, $d_2 = 758.448$, $c_3 = 3.80018 \times 10^{-13}$, and $d_3 = 23.763$. Similarly, for the radiative association process ($d^3\Pi \rightarrow a^3\Pi$), the values are $a = 1.90925 \times 10^{-15}$, $x = 0.3638$, $c_1 = 3.05111 \times 10^{-10}$, $d_1 = 7875.53$, $c_2 = -4.15024 \times 10^{-12}$, $d_2 = 427.166$, $c_3 = 0$, and $d_3 = 0$. These parameters fit the data listed in Table 3 to better than ten percent across the temperature range from 10 to 10000 K.

4 DISCUSSION

We assessed the radiative association process for the possible triplet state transitions yielding CH^+ . The rate coefficients will be dominated by the $d^3\Pi$ to $a^3\Pi$ cross sections and their values for radiative association (2) were calculated. The rates for the $d^3\Pi \rightarrow a^3\Pi$ transition decrease from about $6.5 \times 10^{-15} \text{ cm}^3/\text{s}$ at 10 K to about $6.6 \times 10^{-16} \text{ cm}^3/\text{s}$ at 10000 K.

In our analysis, we ignored the effects of the spin-orbit

splitting of the $\text{C}(^3\text{P})$ atom and the consequent fine structure splittings of the $d^3\Pi$ state and $b^3\Sigma^-$ state (Sarre & Whitham 1988) and their rotational coupling (Stancil et al. 1998a), which may affect the validity of our results for low temperatures. However, in the cold interstellar medium the $\text{C}(^3\text{P})$ atoms will be in the lowest level of the lowest term (Bates 1951), which correlates with the $d^3\Pi$ state (Gentry & Giese 1977), making it likely that the main channel for the radiative association process (2) will be via the $d^3\Pi \rightarrow a^3\Pi$ transition. The chance that the $\text{C}(^3\text{P})$ atom and H^+ ion come together in the $d^3\Pi$ state, which we assumed to be $\frac{2}{3}$, would need to be adjusted accordingly.

In most astrophysical environments where formation of CH^+ is modeled, the carbon atoms are ionized before hydrogen atoms, hence the process (1) is dominant, when it is important, where the rate coefficients for the $\text{A}^1\Pi \rightarrow \text{X}^1\Sigma^+$ transition are around $2 \times 10^{-17} \text{ cm}^3/\text{s}$ at 1000 K (Graff et al. 1983; Barinovs & van Hemert 2006). Thus, while process (2) is faster than (1), its relevance will depend on the relative concentration of C versus $\text{C}^+(^2\text{P}^0)$.

5 SUMMARY AND CONCLUSIONS

The rate coefficients for the radiative association process (2) were calculated and found to be about 100 times larger than those for (1), though applicability would require an environment where neutral carbon exists in the presence of protons, which is the reverse of the usual case. An application might be to modeling the variation of the emission of atomic carbon with the cosmic ionization rate in metal-poor galaxies (Glover & Clark 2016).

ACKNOWLEDGEMENTS

ITAMP is supported in part by a grant from the NSF to the Smithsonian Astrophysical Observatory and Harvard University. BMMcL acknowledges support from the ITAMP visitor's program and from Queen's University Belfast for the award of a Visiting Research Fellowship (VRF). Grants of computational time at the National Energy Research Scientific Computing Center (NERSC) in Berkeley, CA, USA and at the High Performance Computing Center Stuttgart (HLRS) of the University of Stuttgart, Stuttgart, Germany are gratefully acknowledged. This research made use of the NASA Astrophysics Data System.

REFERENCES

- Babb J. F., McLaughlin B. M., 2017, *J. Phys. B: At. Mol. Opt. Phys.*, 50, 044003
 Bacchus-Montabonel M.-C., Wiesenfeld L., 2013, *Chem. Phys. Lett.*, 583, 23
 Barinovs Ģ., van Hemert M. C., 2004, *Chem. Phys. Lett.*, 399, 406
 Barinovs Ģ., van Hemert M. C., 2006, *ApJ*, 636, 923
 Bates D. R., 1951, *MNRAS*, 111, 303
 Biglari Z., Shayesteh A., Maghari A., 2014, *Comp. Theo. Chem.*, 1047, 22
 Black J. H., Dalgarno A., 1973, *Astrophys. Lett.*, 15, 79
 Black J. H., Dalgarno A., 1977, *ApJS*, 34, 405

- Cecchi-Pestellini C., 2010, in Babb J. F., Kirby K., Sadeghpour H., eds, Proceedings of the Dalgarno Celebratory Symposium. Imperial College Press, London, p. 173
- Cho Y.-S., Le Roy R. J., 2016, *J. Chem. Phys.*, **144**, 024311
- Cooley J. W., 1961, *Math. Comput.*, **15**, 363
- Cooper D. L., Kirby K., Dalgarno A., 1984, *Can. J. Phys.*, **62**, 1622
- Cowan R. D., 1981, The Theory of Atomic Structure and Spectra. University of California Press, Berkeley, California, USA
- Curtis L. J., 2003, Atomic Structure and Lifetimes: A Conceptual Approach. Cambridge University Press, Cambridge, UK
- Dalgarno A., Black J. H., 1976, *Rep. Prog. Phys.*, **39**, 573
- Elander N., Oddershede J., Beebe N. H. F., 1977, *ApJ*, **216**, 165
- Gentry W. R., Giese C. F., 1977, *J. Chem. Phys.*, **67**, 2355
- Giusti-Suzor A., Roueff E., van Regemorter H., 1976, *J. Phys. B: At. Mol. Opt. Phys.*, **9**, 1021
- Glover S. C. O., Clark P. C., 2016, *MNRAS*, **456**, 3596
- Graff M. M., Moseley J. T., Roueff E., 1983, *ApJ*, **269**, 796
- Green S., Bagus P. S., Liu B., McLean A. D., Yoshimine M., 1972, *Phys. Rev. A*, **5**, 1614
- Hakalla R., Kepa R., Szajna W., Zachwieja M., 2006, *Eur. Phys. J. D.*, **38**, 481
- Hechtfischer U., Rostas J., Lange M., Linkemann J., Schwalm D., Wester R., Wolf A., Zajfman D., 2007, *J. Chem. Phys.*, **127**, 204304
- Indriolo N., Oka T., Geballe T. R., McCall B. J., 2010, *ApJ*, **711**, 1338
- Johnson B. R., 1977, *J. Chem. Phys.*, **67**, 4086
- Kanzler A. W., Sun H., Freed K. F., 1991, *Int. J. Quant. Chem.*, **29**, 269
- Knowles P. J., Werner H.-J., 1985, *Chem. Phys. Lett.*, **115**, 259
- Kowalski K., Piecuch P., 2001, *Chem. Phys. Lett.*, **347**, 237
- Langhoff S. R., Davidson E. R., 1974, *Int. J. Quantum Chem.*, **8**, 61
- Levy B., Ridard J., Le Coarer F., 1985, *Chem. Phys.*, **92**, 295
- Morris P. W., et al., 2016, *ApJ*, **829**, 15
- Mott N. F., Massey H. S. W., 1965, The Theory of Atomic Collisions, 3rd edn. Clarendon Press, Oxford, UK
- Nagy Z., et al., 2013, *A&A*, **550**, A96
- Novotný O., et al., 2013, *ApJ*, **777**, 54
- Nyman G., Gustafsson M., Antipov S. V., 2015, *Int. Rev. Phys. Chem.*, **34**, 385
- O'Connor A. P., et al., 2016, *Phys. Rev. Lett.*, **116**, 113002
- Sarre P. J., Whitham C. J., 1988, *Chem. Phys.*, **124**, 439
- Sauer S. P. A., Špirko V., 2013, *J. Chem. Phys.*, **138**, 024315
- Saxon R. P., Liu B., 1983, *J. Chem. Phys.*, **78**, 1344
- Saxon R. P., Kirby K., Liu B., 1980, *J. Chem. Phys.*, **73**, 1873
- Seleznev A. O., Khrustov V. F., 2012, *Russ. J. Phys. Chem. B*, **6**, 681
- Seleznev A. O., Khrustov V. F., Stepanov N. F., 2013, *Chem. Phys. Lett.*, **588**, 253
- Smith W. H., Liszt L. S., Lutz B. L., 1973, *ApJ*, **183**, 69
- Solomon P. M., Klemperer W., 1972, *ApJ*, **178**, 389
- Stancil P. C., Babb J. F., Dalgarno A., 1993, *ApJ*, **414**, 672
- Stancil P. C., et al., 1998a, *J. Phys. B: At. Mol. Opt. Phys.*, **31**, 3647
- Stancil P. C., et al., 1998b, *ApJ*, **502**, 1006
- Stecher T. P., Williams D. A., 1974, *MNRAS*, **168**, 51P
- Talbi D., DeFrees D. J., 1991, *Chem. Phys. Lett.*, **179**, 165
- Tielens A., 2005, The Physics and Chemistry of the Interstellar Medium. Cambridge University Press, Cambridge
- Vissapragada S., Buzard C. F., Miller K. A., O'Connor A. P., de Ruelle N., Urbain X., Savin D. W., 2016, *ApJ*, **832**, 31
- Watson J. K. G., 2008, *J. Molec. Spectrosc.*, **253**, 5
- Werner H.-J., Knowles P. J., 1985, *J. Chem. Phys.*, **82**, 5053
- Werner H.-J., Knowles P. J., Knizia G., Manby F. R., Schütz M., et al., 2015, MOLPRO, version 2015.1, a package of *ab initio* programs
- Williams D. A., 1992, *Planet. Space. Sci.*, **40**, 1683

This paper has been typeset from a $\text{\TeX}/\text{\LaTeX}$ file prepared by the author.